Journal of Materials Chemistry B

Accepted Manuscript

ROYAL SOCIETY OF CHEMISTRY

www.rsc.org/materialsB

Novel Ag/Au/Pt trimetallic nanocages used with surface-enhanced Raman scattering for trace fluorescent dye detection

Tran Thi Bich Quyen[a], Wei-Nien Su[b,*], Ching-Hsiang Chen[a, c], John Rick[a], Jyong-Yue Liu[a], Bing-Joe Hwang[a,d,*]

[a]Nanoelectrochemistry Laboratory, Department of Chemical Engineering, National Taiwan University of Science and Technology, Taipei 106, Taiwan

[b]Graduate Institute of Applied Science and Technology, National Taiwan University of Science and Technology, Taipei 106, Taiwan

[c]Protrustech Corporation Limited, 3F.-1, No.293, Sec. 3, Dongmen Rd. East District, Tainan, 701, Taiwan.

[d]National Synchrotron Radiation Research Center, Hsinchu 30076, Taiwan

***Corresponding Authors:** (1) Bing-Joe Hwang: E-mail:bjh@mail.ntust.edu.tw and (2) Wei-Nien Su: E-mail: wsu@mail.ntust.edu.tw

ABSTRACT

Trimetallic nanostructures have received considerable attention in recent years, due to their widespread use in photonics, catalysis, and surface-enhanced Raman scattering (SERS) detection. Nanoparticles consisting of multiple ($n \geq 3$) noble metal components, synthesized under controlled conditions, show better SERS-active stability than mono- or bimetallic nanoparticles. In this work, a simple and novel protocol was used for the synthesis of hollow or porous Ag/Au/Pt trimetallic nanocages, based on a galvanic replacement reaction and co-reduction of the corresponding ions. The nanocages were characterized by UV–vis spectroscopy, transmission electron microscopy (TEM), high-resolution TEM, and X-ray diffraction. It was also demonstrated that the Ag/Au/Pt trimetallic nanocages were both extremely SERS-active and stable. Our results show that Rhodamine 3B, used as a fluorescent marker, could be detected over a wide concentration range from 10^{-15} to 10^{-8} M, with the lower limit of detection being 10^{-15} M.

KEYWORDS. Surface-enhanced Raman scattering; Ag nanocubes; Ag/Au/Pt trimetallic nanocages; Rhodamine 3B; trimetallic nanocages

1. INTRODUCTION

In recent years, assemblies of bimetallic or trimetallic noble metal (Ag, Pt, Au, Ru, and Rh) nanoparticles have played a more prominent role in catalysis. The use of a second and/or third metal not only leads to changes in the particle's physical and chemical properties, e.g. size, shape, surface morphology, catalytic activity and selectivity; but, also results in new properties and capabilities, due to inter-metallic synergies.[1-11] Recently, surface-enhanced Raman scattering (SERS) has attracted considerable interest because of its potential for trace chemical analysis.[12, 13] SERS on rough metal substrates, especially on Ag, Au, and Cu, provides a powerful means of obtaining sensitive frequency resolved vibrational information, related to adsorbate–surface interactions, from high intensity scattering.[14, 15] The SERS signal intensity can be affected by both electromagnetic enhancement and chemical enhancement. Chemical enhancement arises through electronic resonance and charge transfer, between a molecule and a metal surface, resulting in an increase in molecular polarizability. Electromagnetic enhancement, which is usually stronger, takes place under conditions of surface plasmon excitation. The effect of an electromagnetic field is greatly enhanced by amplification of both the incident laser field and the scattered Raman field through surface interactions.

The frequency of the local surface plasmon resonance (LSPR), for noble metals such as Ag, Au, and Pt that exhibit excitation by incident light, or for bi- or trimetallic nanostructures can be tuned: for example a strong enhancement to the SERS effect is observed with nanostructured ensembles of free-electron possessing metals (e.g. the noble metals Au, Ag, and Cu), bimetallic alloys and core/shell nanostructured materials.[16, 17] Bimetallic nanostructures e.g. Pt-Ag nanoparticles, Au-Ag nanoporous nanotubes and Cu-Au nanotubes, provide a significant SERS enhancement[18-20] - as a result, functionalized and conjugated nanostructures, formed on Ag or Au nanoparticles, have gained much attention.[21-23] Anisotropic nanomaterials, e.g. nanocages and nanocubes, possessing sharp features that increase the contribution made by electromagnetic enhancement, especially those from transverse and

longitudinal polarizations, have enhanced plasmon modes[24-27] which result in SERS enhancement factors greater than those associated with spherical nanoparticle's .[28]

Although the rational design and synthesis of multi-metallic nanoparticle's remains problematic, nanostructured design can help give higher stability in comparison to mono-metallic nanoparticles, thereby potentially overcoming problems such as the susceptibility of Cu and Ag to oxidation in air.[29] Recently, diverse Pd/Ag/Rh trimetallic nanoparticles with unique large surface-to-volume ratios have been synthesized for use in catalysis.[30] Furthermore, Ag/Au/Pt trimetallic nanoparticles, which allow the LSPR to be compositionally tuned in a continuous manner, have been investigated.[31, 32] However, the potential of stable Ag/Au/Pt trimetallic structures, formed as nanocages (NCs), has not yet been explored and reported. In this work, we used a modified method to prepare Ag nanocubes[33] - after which, Ag/Au/Pt nanocages were prepared by a galvanic replacement reaction. Although Au and Pt are expensive, the formation of porous structures, after combining with Ag, allows for a significant reduction in material costs.

2. EXPERIMENTAL DETAILS

2.1. Materials

Ethylene glycol (EG), silver nitrate ($AgNO_3$), poly(*N*-vinylpyrrolidone) (PVP; $M_W \approx 55{,}000$), Rhodamine 3B (Rd3B; ≥99%), hydrogen tetrachloroaurate ($HAuCl_4.3H_2O$; ≥ 99.99%), hydrochloric acid (HCl; 36-37%), sodium borohydride ($NaBH_4$), ethanol (C_2H_5OH: ≥ 99.5%), acetone (CH_3COCH_3: ≥99.5%), and chloroplatinic acid hexachloroplatinate ($H_2PtCl_6.6H_2O$; ≥37.5% Pt basis) were all purchased from either Acros or Sigma-Aldrich. All solutions were prepared using deionized water from a MilliQ system.

2.2. Nanocage synthesis

2.2.1. Preparation of silver nanocubes

Silver nanocubes were synthesized using modifications to a previously reported method.[33] Normally, Ag nanocube synthesis requires long reaction times, e.g. to obtain cubes of 30 nm edge length approximately 15 h, and cubes of 130 nm edge length approximately 26 h.[33] Here, in a 100-mL round-bottomed flask, EG (5 mL) was heated at 140°C in an oil bath with magnetic stirring for 40 min. Next, solutions of the following reagents were added by a micropipette in succession: 1) $NaBH_4$ (10 mM in EG; 20 μL); 2) after 2 min, quickly, HCl (3 mM in EG; 1 mL); 3) after another 10 min, at a rate of 45 mL/h, $AgNO_3$ (94 mM in EG; 3 mL) and PVP (147 mM (based on the repeating unit) in EG; 3 mL). Upon injection of the $AgNO_3$ solution, the reaction mixture changed color from milky white, through transparent light yellow and red to ochre, while being heated at 140°C. After 5 h, the solution was centrifuged (10000 rpm; 15 min), the precipitated Ag nanocubes were washed with acetone, ethanol and then H_2O to remove excess EG and PVP, prior to being re-dispersed in deionized water. The average edge length of the Ag nanocubes, as determined from TEM images, was ~70 nm.

2.2.2. Synthesis of Ag/Au/Pt trimetallic nanocages

Typically, a Ag nanocube suspension, as prepared above (100 μL), was dispersed in H_2O (5 mL) containing PVP (1 mg/mL) with stirring and heated at boiling point for 10 min. A $HAuCl_4$ solution (1 mM in H_2O, 1.0 mL) was added to the flask using a syringe pump, at a rate of 45 mL/h, with stirring. After completion of the addition, the mixture was heated for another 10 min, and then H_2PtCl_6 solution (5 mM in H_2O; 350 μL) was added. The mixture was heated for another 10 min until the color was stable. After cooling to room temperature and centrifugation (10000 rpm), the precipitated Ag/Au/Pt trimetallic nanocages (NCs) were washed first with brine to remove AgCl and then repeatedly with deionized water to remove PVP and NaCl. The NCs were re-dispersed in deionized water (1.0 mL) for the SERS study.

2.3. Characterization

Particle solution UV–Vis (absorbance) spectra were acquired on a Shimadzu UV-675 spectrophotometer. Transmission electron microscopy (TEM) was performed on a Philips Tecnai F20 G2 FEI-TEM microscope (accelerating voltage 200 kV). Energy Dispersive X-ray (EDX) measurements were performed on a JSM 6500 EDX analyzer. Specimens were prepared by dropping onto a copper grid and drying at 60°C in an oven. The powder X-ray diffraction (XRD) patterns of the Ag nanocube and Ag/Au/Pt trimetallic NC samples were acquired on a Rigaku Dmax-B diffractometer with a Cu Kα source operated at 40 kV and 100 mA. A scan rate of 0.05 deg^{-1} was used, for 2θ, between 30° and 90°. Raman measurements were performed on a ProMaker confocal Raman microscope system, integrated by the Protrustech Corp., Ltd, Taiwan. A solid state laser operating at λ = 532 nm was used as the excitation source with a laser power of 20 mW. All Raman spectra were obtained with 10 s exposure time. The laser line was focused onto the sample in backscattering geometry using a 50x objective lens providing exciting area of ~4 um^2.

2.4. Preparation of SERS substrates

Droplets (50 μL of a 1.18×10^{10} particle mL^{-1} solution) of Ag/Au/Pt NC were spread on silicon wafers (~1 cm^2). Aqueous Rd3B solution (10^{-8} M; 5 μL droplets) was spread on the Ag/Au/Pt NC surfaces and kept in the dark for 1 h at room temperature prior to testing. For Rd3B quantification, samples with concentrations of 10^{-8}, 10^{-10}, 10^{-12}, 10^{-13}, 10^{-14}, and 10^{-15} M were used. SERS spectra for all samples were measured in triplicate, within 10 min, over 3 different areas on the sample focus at 25°C. The measurements were found to be reproducible within acceptable measurement errors.

3. RESULTS AND DISCUSSION

3.1. Characterization of the Ag nanocubes and Ag/Au/Pt trimetallic nanocages

The UV-Vis spectra of Ag nanocubes (70 nm edge length) showed a main broad band with a maximum at 456 nm and a shoulder at 348 nm. Figure 1 shows the solution absorbance spectra of Ag/Au/Pt nanocages (NCs) prepared with Ag:Au:Pt weight ratios of 0.89:0.065:0.045, 0.63:0.16:0.21, and 0.57:0.20:0.23. During the preparation of Ag/Au/Pt trimetallic NCs, the position of the SPR peak continuously shifted from the visible (~456 nm for the Ag nanocubes) to the near-infrared (~725 nm) when $HAuCl_4$ solution was added into the Ag nanocube solution (spectrum b in Figure 1). The absorption peak of Ag/Au/Pt NCs was blue-shifted from 725 to 653 nm and then gradually disappeared with increasing contents of Au and Pt (spectra c & d in Figure 1). It is interesting to note that Pt shows no strong characteristic absorption over the entire spectral range.

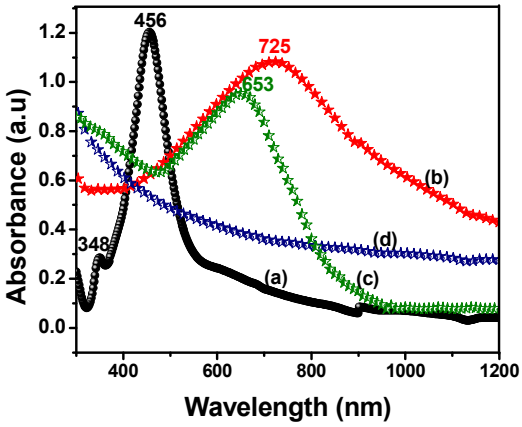

Figure 1. UV-vis spectra of: (a) Ag nanocubes (~70 nm); and Ag/Au/Pt NCs with weight ratios of Ag:Au:Pt of (b) 0.89:0.065:0.045; (c) 0.63:0.16:0.21; and (d) 0.57:0.20:0.23.

Figure 2 shows representative TEM images of Ag nanocubes and Ag/Au/Pt NC samples. The addition of small amounts of $NaBH_4$ and HCl can significantly reduce the synthesis time to about 5 h. The reducing agents increased the rate of Ag^+ reduction, leading to smooth nucleation and the formation of uniform Ag nanocube particles, as seen Figure 2(a). The images of the trimetallic NCs in

Figures 2(b)-(d) reveal that the porous nanocage structure has been preserved during the galvanic replacement process, indicating a direct replacement of Ag atoms ($Ag^{(0)}$) with Au and Pt atoms ($Au^{(0)}$ and $Pt^{(0)}$) upon addition of $HAuCl_4$ and H_2PtCl_6. There is a clear contrast between the interior and exterior of the NCs in the TEM image (Figure 2(c)), indicating a hollow or porous interior structure. Figure 2(e) shows the HR-TEM image of Ag/Au/Pt trimetallic NCs from Figure 2(c). The outer shell and the porous interior can be easily distinguished by variations in the image contrast and fringe. The measured lattice spacings i.e. 0.419, 0.402, and 0.241 nm match the structures of Ag, Au, and Pt, respectively. The result implies that the Ag, Au, and Pt were successfully combined in one NC after galvanic replacement. EDX analysis shows the presence of Ag, Au, and Pt at 63.172 16.188, and 20.640 wt%, respectively. Hence, the formation of trimetallic nanocages in the atomic ratio of Ag:Au:Pt = 0.76:0.14:0.10 was confirmed by EDX, as shown in Figure S1 (Supporting Information).

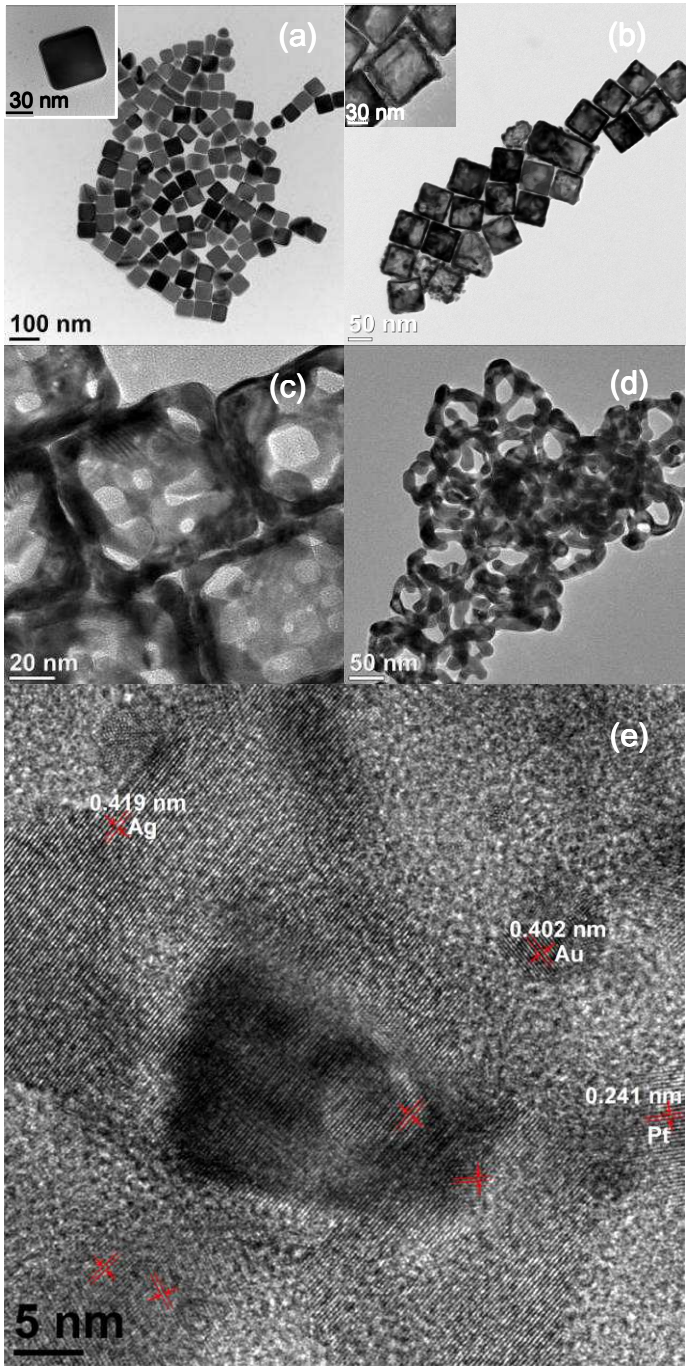

Figure 2. TEM images of: (a) Ag nanocubes (~70 nm) and Ag/Au/Pt NCs with weight ratios of Ag:Au:Pt of (b) 0.89:0.065:0.045; (c) 0.63:0.16:0.21; and (d) 0.57:0.20:0.23. (e) HRTEM image of Ag/Au/Pt NCs at a ratio of Ag:Au:Pt of 0.63:0.16:0.21. (enlarged view of (c))

The X-ray diffraction (XRD) patterns of Ag nanocubes and Ag/Au/Pt NCs are shown in Figure 3. The diffraction peaks located at 38.1°, 44.3°, 64.7°, 77.6° and 81.9° can be indexed to the (111), (200), (220), (311), and (222) planes, of the face-centered cubic (fcc) structures of Ag, Au, and Pt (JCPDS No. 87-0720, 04-0784 and 87-0647) respectively. The peaks of Ag and Au almost overlap, but at 77° the peak from Ag/Au/Pt NCs shows a clear shift towards a higher angel. That may be attributed to lattice strain resulting from the presence of Au, present as an external shell-layer on the Ag nanocubes, before Ag replacement. The diffractograms, for the Ag/Au/Pt NCs sample, show the peaks at (111), (220) and (311) have a shoulder when compared to Ag nanocubes. The crystallographic surface marked for Pt (2θ = 40.25, 65.36, 78.62), indicates the formation of Ag/Au/Pt trimetallic NCs. The (200) peak of the Ag/Au/Pt sample is more intense than the (111) peak that dominates the JCPDS pattern, mainly because the cubes are joined at the {100} facets, whereas the powder standard is overwhelmed by the lower energy {111} facets. This indicates that most nanocages are aligned flat on the substrate with their {100} planes being oriented upward.

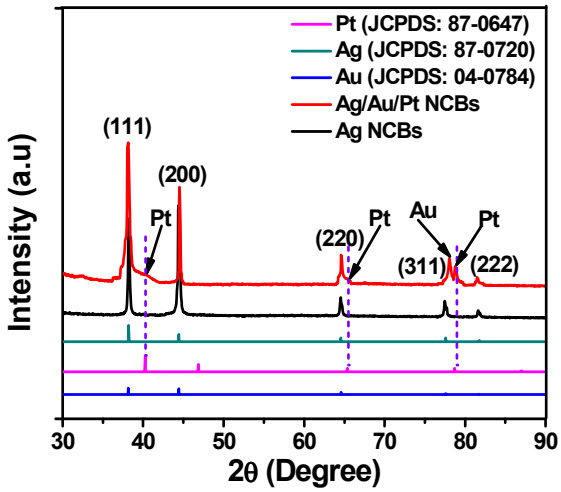

Figure 3. XRD patterns of Ag nanocubes and Ag/Au/Pt NCs at ratio of Ag:Au:Pt = 0.63:0.16:0.21.

3.2. The formation mechanism of the Ag/Au/Pt trimetallic porous nanocages

The proposed mechanism for the growth of Ag/Au/Pt trimetallic nanocages is depicted in Scheme 1. When $AgNO_3$ solution is injected into $HCl/NaBH_4$ solution in EG at 140°C, Ag ions are quickly reduced to form nanocubic $Ag^{(0)}$ by EG and BH_4^-. In the presence of solid Ag, $HAuCl_4$ and H_2PtCl_6 can be reduced to generate Au and Pt atoms by the galvanic replacement reaction in aqueous solution[34, 40] shown in equations (1) and (2). In this case, Ag/Au/Pt porous nanocages are prepared from templates based on Ag nanocubes produced in large quantities by polyol reduction.

$$3Ag(s) + AuCl_4^- \rightarrow Au(s) + 4Cl^-(aq) + 3Ag^+(aq) \qquad (1)$$

$$4Ag(s) + PtCl_6^{2-} \rightarrow Pt(s) + 6Cl^-(aq) + 4Ag^+(aq) \qquad (2)$$

As the reaction proceeds, porous nanocages are formed by replacement interactions between Ag and Au. Upon addition of a H_2PtCl_6 solution to the Ag/Au solution at 140°C, Pt atoms form immediately by galvanic replacement reaction between $Ag^{(0)}$ and Pt ions. The $Ag^{(0)}$ atoms in the nanocubic structure are replaced by Pt and then porous trimetallic Ag/Au/Pt structures forms in a manner similar to Au atoms, as described above.

After Ag nanocubes with sharp corners in Figure 2(a) react with an alternately small amount of $HAuCl_4$ and H_2PtCl_6 solutions, pinholes are first observed on one of six cubic faces, as shown in Figure 2(b), indicating that the reaction begins locally at a high-energy site (e.g, surface step, point defect, or hole in capping layer) rather than over the entire cube.[35] As the reaction proceeds, these pinholes serve as the anode, where Ag is oxidized and electrons are stripped. The released electrons migrate to the nanocube faces and are alternately captured by $AuCl_4^-$ and $PtCl_6^{2-}$, generating Au and Pt atoms that epitaxially grow on the nanocube. As the Au and Pt layers are formed, the initial pinholes or hollows would serve as the sites for Ag dissolution, facilitating the conversion of the nanocube into a nanocage, as seen in Figure 2(c). In later stages of reaction, presumably through mass diffusion processes and/or direct deposition of Au and Pt near the pinholes, larger hollow interior of the nanocage is formed. Finally, the structure of nanocages or nanocubes is likely to deform, when the

amount of $HAuCl_4$ and H_2PtCl_6 added alternately into the Ag nanocube solution exceeds a certain limit, as shown in Figure 2(d).

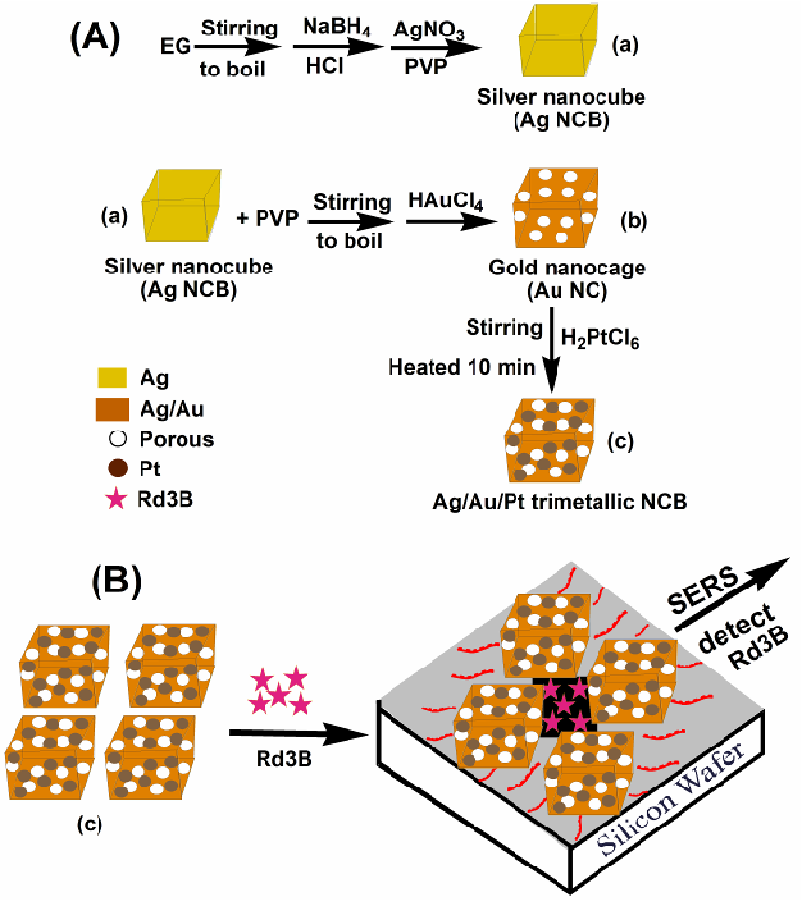

Scheme 1. (A) Showing the synthesis of Ag nanocubes and Ag/Au/Pt trimetallic nanocages, and (B) showing the solution phase agglomeration of Ag/Au/Pt trimetallic nanocages application for SERS in the presence of Rd3B.

3.3. Application of the Ag/Au/Pt trimetallic porous nanocages in SERS measurements

Next, the SERS signal intensity of Rd3B on Ag/Au/Pt NCs with various ratios of Ag:Au:Pt was investigated (Figure 4). Rd3B is an excellent model analyte in SERS studies because it is photostable and lacks absorption in the near-infrared (NIR) region. Figure 4(A) shows a comparison of the SERS intensity of Rd3B.

There was no SERS signal on a silicon substrate (a), whereas the signal was the most intense on Ag/Au/Pt NCs (d) and Ag nanocubes (b). The peak at ~638 cm^{-1} is assigned to the C–H out-of-plane bend mode, the peak at ~1148 cm^{-1} – to the C–H in-plane bend mode and the series of peaks at ~1379, 1528, 1585 and 1667 cm^{-1} – to the aromatic ring vibrational modes of Rd3B. The SERS signal intensity on Ag/Au/Pt NCs was stronger than that on the silicon substrate with an enhancement factor of SERS activity of 4.7×10^{9} (from the spectra (d) and (a)) based on the calculated method[36] by the equation $EF = \frac{(I_{SERS}/C_{SERS})}{(I_{ref}/C_{ref})}$. In this equation, C_{ref} (10^{-1} M) and C_{SERS} represent the concentrations of Rd3B on the silicon substrate, whereas I_{ref} and I_{SERS} represent the signal intensities obtained from Rd3B on the silicon substrate and on Ag/Au/Pt NCs substrate respectively. The pores on the Ag/Au/Pt NC surfaces are expected to contribute to the high SERS activity due to a large electric field enhancement. Also, a significant charge transfer interaction between the ligand and the Pt-coated Ag/Au substrate is expected in view of the difference in electro-negativity of Ag, Au, and Pt.[30] Rd3B on Ag/Au/Pt porous NCs with Ag:Au:Pt ratio of 0.63:0.16:0.21 (The spectrum in 4(d) shows the highest SERS intensity, presumably because the porous structure on the material's surface is suitable for building "hot spots". The SERS intensity of Rd3B decreased gradually when the nanocages on the surface of the material diminished (Figure 2(d) and 4(e)). Comparing Figure 4(c) and 4(d), it seems that Ag:Au:Pt of 0.89:0.065:0.045 has a similar sensitivity to NC 0.63:0.16:0.21, but the former is preferred because Ag is much cheaper than Au and Pt. Herein, we summarize three points which may help explain the significant SERS enhancement of Ag/Au/Pt NCs (with ratios of 0.63:0.16:0.21). First, Ag/Au/Pt NCs are formed when Au and Pt atoms are presented onto Ag nanocubes. It would appear that the quantity and arrangement of these Ag/Au/Pt NCs are optimized when ratio of Ag:Au:Pt = 0.63:0.16:0.21. Second, the redistribution of surface charge, caused by partial electron transfer between Ag, Au and Pt, occurs due to their different work functions. The charge-transfer between Ag, Au and Pt atoms in the trimetallic NCs, creates positively charged domains rich in Ag atoms, and negatively charge regions dominated by

Au and Pt atoms. It is proposed that the probe-specific enhancement is related to the selective binding of probe molecules (i.e, Rd3B) to the partially charged surface domains in the nanocages.[37, 38] Third, the SERS signal intensity and the enhancement factor for Rd3B on Ag/Au/Pt porous nanocages substrate, see spectrum (d), are better than Rd3B on Ag/Au/Pt nonporous nanocages with smooth surfaces – spectrum (c)). As a comparison the SERS enhancement of a nanoporous gold substrate is one to two orders of magnitude greater than that of coarsened smooth surfaced nonporous gold as shown previously.[39]

On the other hand, as more and more Au, Pt atoms form and replace Ag atoms in the nanocage's nanostructure – see Figures 2(e) and 4(d), the area covered by Ag bridge sites will be increasingly interrupted by Au and Pt. The number of adjacent Ag bridge sites will be reduced, dipole-dipole coupling between Rd3B molecules on adjacent Ag bridge sites will be reduced, and the frequency of the Ag bridge-site adsorption band will decrease.[40] Moreover, electron transfer between Ag, Au and Pt can also reduce the amount of Rd3B adsorbed at Ag bridge sites. Therefore, the relative intensity of the 1667 cm^{-1} band will decrease.

The signal intensities of the Ag nanocubes and Ag/Au/Pt NCs [see spectra (b) and (d) in Figure 4(A)] seem comparable, which is interesting as it is known that Ag-Au nanoparticles are much more stable than Ag nanoparticle in air.[29] In Figure 5, the stability of the substrates are compared by repeating the SERS measurements after storage at 4^{o}C for 2 and 45 days respectively. It shows that the SERS signal intensity of Rd3B on Ag nanocubes is significantly reduced to 44.2% of its original value after 45 days, while that of Rd3B on Ag/Au/Pt NCs decreased moderately (only about 15.4%) when compared with samples measured after 2 days. This indicates that the stability of Ag/Au/Pt NCs is much higher than that of Ag nanocubes in the presence of Rd3B, both in air or solution.

To probe the degree of enhancement to the SERS sensitivity of Ag/Au/Pt porous NCs with a Ag:Au:Pt ratio of 0.63:0.16:0.21, various concentrations of Rd3B on the trimetallic nanocages were

tested as seen in Figure 6. A wide range of Rd3B concentrations (10^{-8} – 10^{-15} M) could be effectively detected. The characteristic peak of Rd3B at 1667 cm^{-1} could still be identified even at a concentration as low as 10^{-15} M. These results imply that the Ag/Au/Pt trimetallic NCs can be used for simple and sensitive quantitative detection of biomolecules *in vivo*. To support this claim, we have compiled the analytical parameters, such as the enhancement factor, range of detection, and excitation source, etc., relevant to SERS detection for different nanomaterials summarized in Table 1.

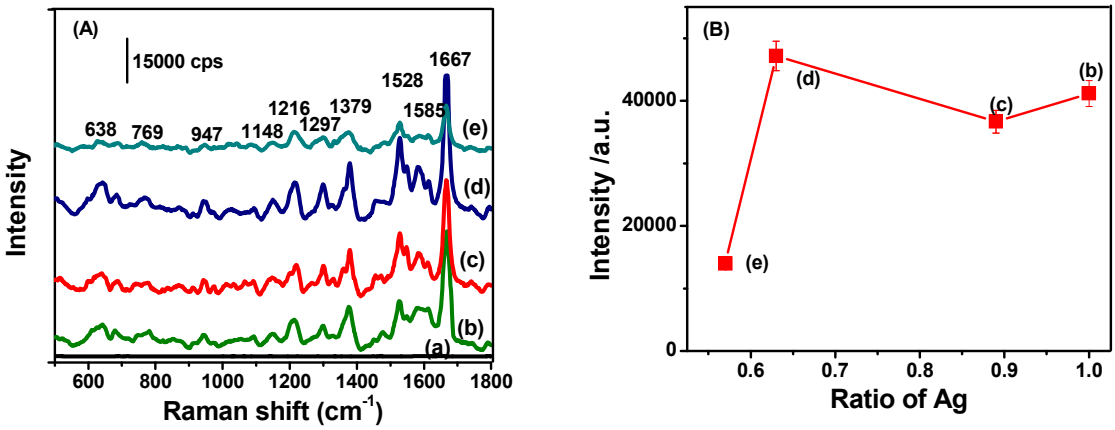

Figure 4. (A) SERS spectra of (a) 100 mM Rd3B on the silicon substrate, 10^{-8} M Rd3B on (b) Ag nanocubes and on Ag/Au/Pt NCs with ratios of Ag:Au:Pt at (c) 0.89:0.065:0.045, (d) 0.63:0.16:0.21, and (e) 0.57:0.20:0.23. (B) Plot with various ratios of Ag:Au:Pt (b-e) vs. signal intensity of Rd3B for the band at 1667 cm^{-1}. Each data point represents an average value from three SERS spectra. Error bars show standard deviations.

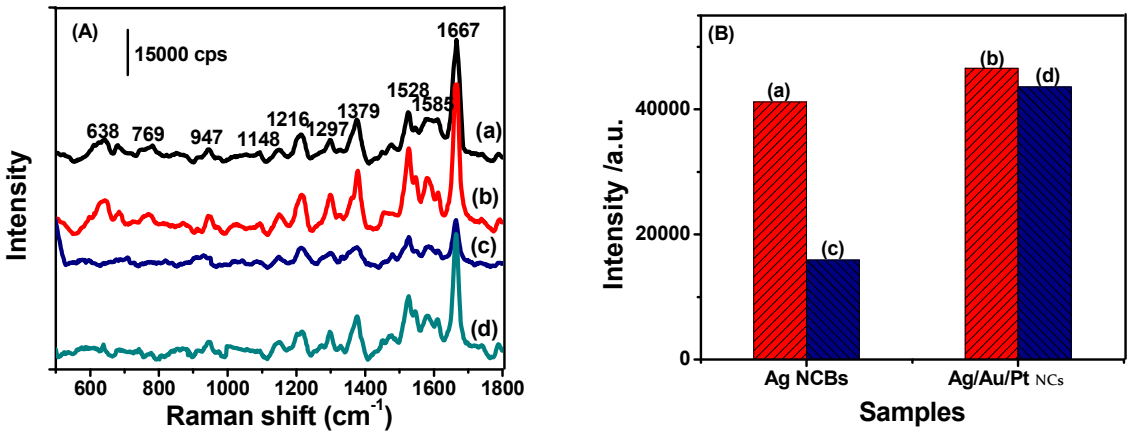

Figure 5. (A) Representative SERS spectra of 10^{-8} M Rd3B on (a, c) Ag nanocubes and (b, d) Ag/Au/Pt NCs (ratio of 0.63:0.16:0.21) were stored at 4°C after 2 days and 45 days, respectively. (B) Stability tests by verifying the signal intensity for the band at 1667 cm^{-1} of Rd3B with time. Each data point represents the average value from three SERS spectra.

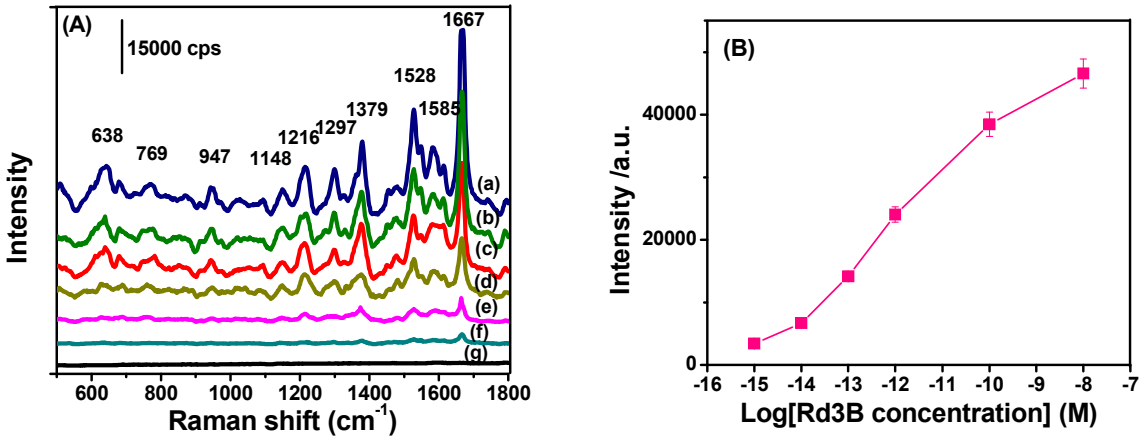

Figure 6. (A) Representative SERS spectra of Rd3B on Ag/Au/Pt NCs at concentrations of: (a) 10^{-8} M; (b) 10^{-10} M; (c) 10^{-12} M; (d) 10^{-13} M; (e) 10^{-14} M; (f) 10^{-15} M; and (g) 0 M. (B) A logarithmic plot of Rd3B concentration vs. signal intensity for the band at 1667 cm^{-1}. Each data point represents an average value from three SERS spectra. Error bars show standard deviations.

Table 1. A summary of the application of various materials in SERS

Material composition	*Detected concentration*	*Molecule Analyte or cell detected*	*SERS enhancement factor*	*Laser excitation, (nm)/source power, (mW)*	*Ref.*
Au_{oct}@PdPt (1) Au_{sph}@PdPt (2) Dendritic Pd-Pt alloy NPs (3)	Not given	4-NBT	(1) > (2) > (3) 2 and 4 times larger	632.8/4.25	Kang et al. [41]
Au@Pd@Pt NPs (molar ratio Au: Pd: Pt = 100: 6:1)	Not given	CO	Not given	632.8/4	Fang et al. [42]
Au-Ag/Ag-Au NPs (alloy and core-shell)	0.5 mM	1,10-phenanthroline	Not given	633/20	Pande et al.[43]
Ag@SiO_2 NPs		R6G	10^5	514.5/not given	Liu et al. [44]
AgM (M=Pt, Pd, Au) NPs	10 nM	R6G	Not given	633/2.5	Chen et al. [45]
Cu-Au alloy NTs	1 μM	4-Mpy	3 times larger than that on Cu nanowires	638/11.9	Jiang et al. [20]
Cu-Zr amorphous alloys	0.05 M	Pyridine	Not given	647.1/not given	Kudelski et al. [46]
Au/Pt/Ag trimetallic NPs (atomic ratio Au : Pt : Ag = 1 :2 :1)	Not given	7-azaindole	Not given	1064/not given	Karthikeyan et al.[32]
Au/SiO_2 composite NPs	2×10^{-5} M	R6G	3 times larger than that on Au substrate	633/1	Liu et al. [47]
Ag/SiO_2 composite NPs	2×10^{-6} M	R6G	3 times larger than that on Ag substrate	514/1	Liu et al. [48]
Au nanochains	5 nM	R6G	10^7 - 10^9	532/40	Polavarapu et al. [49]
Au@SiO_2@Ag NPs	1 μM	RdB	1.03×10^5	785/25-500	Li et al. [15]
AgFON/EG3	(0-450 mg/dL, 0-25 mM)	Glucose	Not given	632.8/5	Yonzon et al. [50]
Au colloidal solution	2.9 mg/dL	Uric acid	Not given	785/120	Premasiri et al. [51]
Au@SiO_2 NPs	10^{-7} M; 10^{-3}-10^{-12} M; 1.72×10^{-4}-10^{-11} M	R6G; Glucose; and Uric acid	1.2×10^8	532/20	Quyen et al.[52]
Au@SiO_2 NRs	10^{-8}-10^{-16} M; 10 ng/mL-0.86 fg/mL	R6G; CEA antigen	3.6×10^9	532/20	Quyen et al. [53]
Ag/Au/Pt NCs	10^{-8}-10^{-15} M	Rd3B	4.7×10^9	532/20	This work

Figure 7 shows an SEM image and SERS mapping of Ag/Au/Pt NCs in the presence of Rd3B molecules. The distribution of Rd3B molecules on Ag/Au/Pt NCs (scan area: 20 × 20 μm^2) is illustrated, based on the highest signal intensity of peak at 1667 cm^{-1}. It should be noted that the

uniform distribution of the Rd3B characteristic peak signals represents a uniform distribution on the Ag/Au/Pt NCs substrate in this wavenumber region – this is attributed to the self-assembled structures that greatly enhance the reliability of the measurements, as seen in the SERS mapping, Figure 7(B).

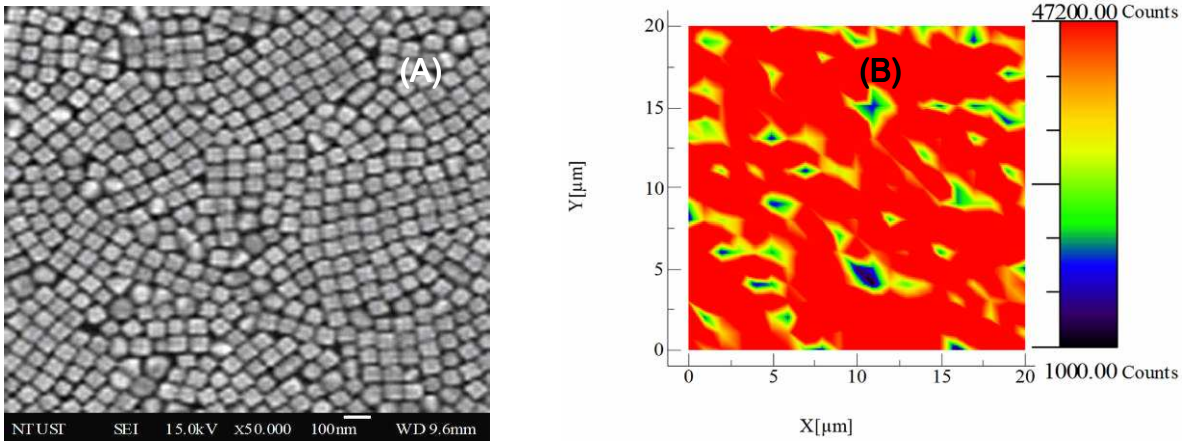

Figure 7. (A) SEM image of 10^{-8} M Rd3B on Ag/Au/Pt NC (weight ratio Ag:Au:Pt of 0.63:0.16:0.21). (B) SERS mapping of Rd3B on Ag/Au/Pt NCs based on the most intense peak (1667 cm^{-1}). This image is a 2D projection (scan area 20 × 20 μm^2).

4. CONCLUSIONS

This work describes a simple method for the synthesis of Ag/Au/Pt trimetallic porous nanocages (Ag/Au/Pt NCs) using a galvanic replacement reaction. The nanocages, which possess inter-metallic synergies between Ag, Au and Pt, are able to generate significant SERS signal enhancements, due to "hot spot" formation. Rhodamine 3B can be detected in the concentration range 10^{-8} to 10^{-15} M, with the lower limit of detection being 10^{-15} M. It was also demonstrated that the nanocages can be tailored for SERS applications due to their stability in air, relatively low cost, the convenience for building "hot spots". The strong electronic effects, attributable to the materials' surfaces, significantly increase SERS-active enhancement and thus enable the detection of trace amounts of selected molecular species.

It is anticipated that the strategy demonstrated here may also apply to the synthesis of other bi- or tri-metallic porous nanostructures or core/shell nanostructures.

ACKNOWLEDGEMENT

Financial support from the Ministry of Science and Technology (MoST) (grants 101-3113-E-011-002 and 101-2923-E-011-001-MY3) and the Top University Projects of Ministry of Education (MOE) (grant 103H451401) are acknowledged.

Supporting Information. EDX spectrum of Ag/Au/Pt NCs with a ratio of Ag:Au:Pt = 0.63:0.16:0.21. This material is available free of charge from the Internet.

References

1. D. Wang and Y. Li, *Adv. Mater.*, 2011, **23**, 1044-1060.
2. Z. Chuan-Jian, L. Jin, F. Bin, N. W. Bridgid, N. N. Peter, L. Rameshwori and Y. Jun, *Nanotechnology*, 2010, **21**, 062001.
3. L. Liu and E. Pippel, *Angew. Chem. Int. Ed.*, 2011, **50**, 2729-2733.
4. V. R. Stamenkovic, B. Fowler, B. S. Mun, G. Wang, P. N. Ross, C. A. Lucas and N. M. MarkoviÄ‡, *Science*, 2007, **315**, 493-497.
5. C. Zhu, S. Guo and S. Dong, *Adv. Mater.*, 2012, **24**, 2326-2331.
6. L. Zhang, J. Zhang, Z. Jiang, S. Xie, M. Jin, X. Han, Q. Kuang, Z. Xie and L. Zheng, *J. Mater. Chem.*, 2011, **21**, 9620-9625.
7. F. Meng and Y. Ding, *Adv. Mater.*, 2011, **23**, 4098-4102.
8. H. Bönnemann and Ryan M. Richards, *Eur. J. Inorg. Chem.*, 2001, **2001**, 2455-2480.
9. P. Venkatesan and J. Santhanalakshmi, *J. Mol. Catal. A-Chem.*, 2010, **326**, 99-106.
10. F. Taufany, C.-J. Pan, H.-L. Chou, J. Rick, Y.-S. Chen, D.-G. Liu, J.-F. Lee, M.-T. Tang and B.-J. Hwang *Chem. Eur. J.*, 2011, **17**, 10724-10735.
11. F. Taufany, C. J. Pan, J. Rick, H. L. Chou, M. C. Tsai, B. J. Hwang, D. G. Liu, J. F. Lee, M. T. Tang, Y. C. Lee and C. I. Chen, *ACS Nano*, 2011, **5**, 9370-9381.
12. P. A. Mosier-Boss and S. H. Lieberman, *Langmuir*, 2003, **19**, 6826-6836.
13. X. Liu, F. Zhang, R. Huang, C. Pan and J. Zhu, *Cryst. Growth Des.*, 2008, **8**, 1916-1923.
14. E. J. S. Bell and M. S. N. Sirimuthu, *Chem. Soc. Rev.*, 2008, **37**, 1012-1024.
15. D. Li, D.-W. Li, Y. Li, J. S. Fossey and Y.-T. Long, *J. Mater. Chem.*, 2010, **20**, 3688-3693.
16. M. Moskovits, eds. K. Kneipp, M. Moskovits and H. Kneipp, Springer Berlin / Heidelberg, 2006, pp. 1-17.
17. M. Fan, F.-J. Lai, H.-L. Chou, W.-T. Lu, B.-J. Hwang and A. G. Brolo, *Chem. Science*, 2013, **4**, 509-515.

18. K. Kim, K. L. Kim and K. S. Shin, *J. Phys. Chem. C*, 2011, **115**, 23374-23380.
19. X. Gu, L. Xu, F. Tian and Y. Ding, *Nano Res.*, 2009, **2**, 386-393.
20. Z. Jiang, Q. Zhang, C. Zong, B.-J. Liu, B. Ren, Z. Xie and L. Zheng, *J. Mater. Chem.*, 2012, **22**, 18192-18197.
21. V. Voliani, S. Luin, F. Ricci and F. Beltram, *Nanoscale*, 2010, **2**, 2783-2789.
22. V. Voliani, F. Ricci, S. Luin and F. Beltram, *Journal of Materials Chemistry*, 2012, **22**, 14487-14493
23. L. Škantárová, A. Oriňák, R. Oriňáková, M. Jerigová, M. Stupavská and D. Velič, *Surf. Interface Anal.*, 2013, **45**, 1266.
24. X. Huang, I. H. El-Sayed, W. Qian and M. A. El-Sayed, *Nano Lett.*, 2007, **7**, 1591-1597.
25. N. J. Durr, T. Larson, D. K. Smith, B. A. Korgel, K. Sokolov and A. Ben-Yakar, *Nano Lett.*, 2007, **7**, 941-945.
26. H. Wang, T. B. Huff, D. A. Zweifel, W. He, P. S. Low, A. Wei and J.-X. Cheng, *Proc. Natl. Acad. Sci. USA*, 2005, **102**, 15752-15756.
27. Z. L. Wang, R. P. Gao, B. Nikoobakht and M. A. El-Sayed, *J. Phys. Chem. B*, 2000, **104**, 5417-5420.
28. M. Rycenga, M. H. Kim, P. H. C. Camargo, C. Cobley, Z.-Y. Li and Y. Xia, *J. Phys. Chem. A*, 2009, **113**, 3932-3939.
29. N. Alissawi, V. Zaporojtchenko, T. Strunskus, I. Kocabas, V. S. K. Chakravadhanula, L. Kienle, D. Garbe-Schönberg and F. Faupel, *Gold Bull.*, 2013, **46**, 3-11.
30. T. Matsushita, Y. Shiraishi, S. Horiuchi and N. Toshima, *Bull. Chem. Soc. Jpn.*, 2007, **80**, 1217-1225.
31. Y. Ji, S. Yang, S. Guo, X. Song, B. Ding and Z. Yang, *Colloids Surf., A*, 2010, **372**, 204-209.
32. B. Karthikeyan and B. Loganathan, *Mater. Lett.*, 2012, **85**, 53-56.
33. S. H. Im, Y. T. Lee, B. Wiley and Y. Xia, *Angew. Chem. Int. Ed.*, 2005, **44**, 2154-2157.
34. Y. Sun and Y. Xia, *J. Am. Chem. Soc.*, 2004, **126**, 3892-3901.
35. Z. L. Wang, *J. Phys. Chem. B*, 2000, **104**, 1153-1175.
36. E. C. Le Ru, E. Blackie, M. Meyer and P. G. Etchegoin, *J. Phys. Chem. C*, 2007, **111**, 13794-13803.
37. M. Fan, F.-J. Lai, H.-L. Chou, W.-T. Lu, B.-J. Hwang and A. G. Brolo, *Chem. Sci.*, 2012, **4**, 509-515.
38. C. Wang, B. Peng, H.-N. Xie, H.-X. Zhang, F.-F. Shi and W.-B. Cai, *J. Phys. Chem. C*, 2009, **113**, 13841-13846.
39. L. H. Qian, X. Q. Yan, T. Fujita, A. Inoue and M. W. Chen, *Appl. Phys. Lett.*, 2007, **90**, -.
40. C. Wang, D. van der Vliet, K.-C. Chang, H. You, D. Strmcnik, J. A. Schlueter, N. M. Markovic and V. R. Stamenkovic, *J. Phys. Chem. C*, 2009, **113**, 19365-19368.
41. S. W. Kang, Y. W. Lee, Y. Park, B.-S. Choi, J. W. Hong, K.-H. Park and S. W. Han, *ACS Nano*, 2013.
42. P.-P. Fang, S. Duan, X.-D. Lin, J. R. Anema, J.-F. Li, O. Buriez, Y. Ding, F.-R. Fan, D.-Y. Wu, B. Ren, Z. L. Wang, C. Amatore and Z.-Q. Tian, *Chem. Sci.*, 2011, **2**, 531-539.
43. S. Pande, S. K. Ghosh, S. Praharaj, S. Panigrahi, S. Basu, S. Jana, A. Pal, T. Tsukuda and T. Pal, *J. Phys. Chem. C*, 2007, **111**, 10806-10813.
44. T. Liu, D. Li, Y. Zou, D. Yang, H. Li, Y. Wu and M. Jiang, *J. Colloid Interface Sci.*, 2010, **350**, 58-62.
45. L. Chen, J. M. Chabu and Y. Liu, *RSC Adv.*, 2013, **3**, 4391-4399.
46. A. Kudelski, M. Janik-Czachor, M. Varga, M. Dolata, J. Bukowska, Ã. MolnÃ¡r and A. Szummer, *Appl. Catal. A-Gen.* , 1999, **181**, 123-130.
47. Y.-C. Liu, C.-C. Yu and T.-C. Hsu, *J. Raman Spectrosc.*, 2009, **40**, 1682-1686.

48. Y.-C. Liu, K.-H. Yang and T.-C. Hsu, *J. Phys. Chem. C*, 2009, **113**, 8162-8168.
49. L. Polavarapu and Q. H. Xu, *Langmuir*, 2008, **24**, 10608-10611.
50. C. R. Yonzon, C. L. Haynes, X. Zhang, J. T. Walsh and R. P. Van Duyne, *Anal. Chem.*, 2003, **76**, 78-85.
51. W. R. Premasiri, R. H. Clarke and M. E. Womble, *Lasers in Surgery and Medicine*, 2001, **28**, 330-334.
52. T. T. B. Quyen, W.-N. Su, K.-J. Chen, C.-J. Pan, J. Rick, C.-C. Chang and B.-J. Hwang, *J. Raman Spectrosc.*, 2013, n/a-n/a.
53. Q. T. B. Tran, C.-C. Chang, W.-n. Su, Y.-H. Uen, C.-J. Pan, J.-Y. Liu, J. F. Rick, K.-Y. Lin and B. J. Hwang, *J. Mater. Chem. B*.

Table 1. A summary of the application of various materials in SERS

Figure Captions

Figure 1. UV-vis spectra of (a) Ag nanocubes (~70 nm); and Ag/Au/Pt NCs with weight ratios of Ag:Au:Pt of (b) 0.89:0.065:0.045; (c) 0.63:0.16:0.21; and (d) 0.57:0.20:0.23.

Figure 2. TEM images of (a) Ag nanocubes (~70 nm) and Ag/Au/Pt NCs with weight ratios of Ag:Au:Pt of (b) 0.89:0.065:0.045; (c) 0.63:0.16:0.21; and (d) 0.57:0.20:0.23. (e) HRTEM image of Ag/Au/Pt NCs at a ratio of Ag:Au:Pt of 0.63:0.16:0.21. (enlarged view of (c))

Figure 3. XRD patterns of Ag nanocubes and Ag/Au/Pt NCs at ratio of Ag:Au:Pt = 0.63:0.16:0.21.

Figure 4. (A) SERS spectra of (a) 100 mM Rd3B on the silicon substrate, 10^{-8} M Rd3B on (b) Ag nanocubes and on Ag/Au/Pt NCs with ratios of Ag:Au:Pt at (c) 0.89:0.065:0.045, (d) 0.63:0.16:0.21, and (e) 0.57:0.20:0.23. (B) Plot with various ratios of Ag:Au:Pt (b-e) vs. signal intensity of Rd3B for the band at 1667 cm^{-1}. Each data point represents an average value from three SERS spectra. Error bars show standard deviations.

Figure 5. (A) Representative SERS spectra of 10^{-8} M Rd3B on (a, c) Ag nanocubes and (b, d) Ag/Au/Pt NCs (ratio of 0.63:0.16:0.21) were stored at 4^{o}C after 2 days and 45 days, respectively. (B) Stability tests by verifying the signal intensity for the band at 1667 cm^{-1} of Rd3B with time. Each data point represents the average value from three SERS spectra.

Figure 6. (A) Representative SERS spectra of Rd3B on Ag/Au/Pt NCs at concentrations of: (a) 10^{-8} M; (b) 10^{-10} M; (c) 10^{-12} M; (d) 10^{-13} M; (e) 10^{-14} M; (f) 10^{-15} M; and (g) 0 M. (B) A logarithmic plot of Rd3B concentration vs. signal intensity for the band at 1667 cm^{-1}. Each data point represents an average value from three SERS spectra. Error bars show standard deviations.

Figure 7. (A) SEM image of 10^{-8} M Rd3B on Ag/Au/Pt NC (weight ratio Ag:Au:Pt of 0.63:0.16:0.21). (B) SERS mapping of Rd3B on Ag/Au/Pt NCs based on the most intense peak (1667 cm^{-1}). This image is a 2D projection (scan area 20 × 20 μm^2).

Scheme 1. (A) Showing the synthesis of Ag nanocubes and Ag/Au/Pt trimetallic nanocages, and (B) showing the solution phase agglomeration of Ag/Au/Pt trimetallic nanocages application for SERS in the presence of Rd3B.

TOC image

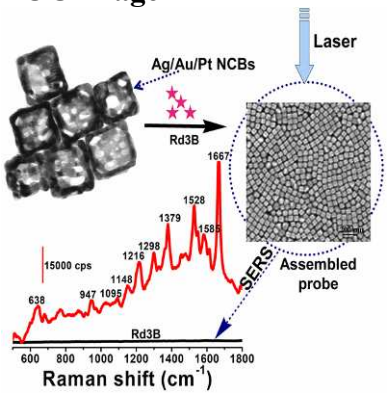

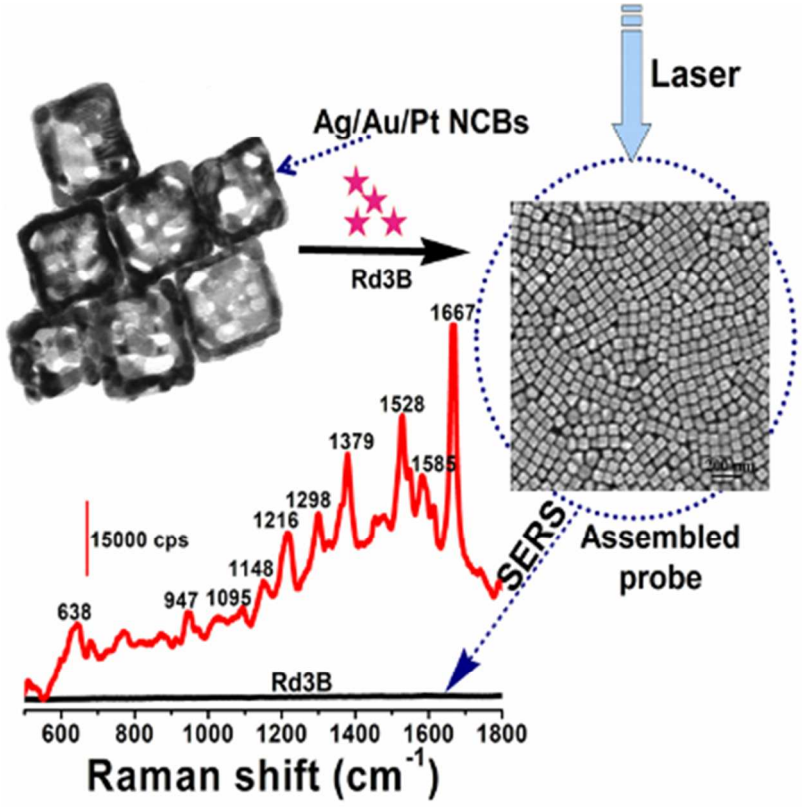

50x50mm (200 x 200 DPI)